Kinesin-mediated Organelle Translocation Revealed by Specific Cellular Manipulations

Fabian Feiguin, Adriana Ferreira,* Kenneth S. Kosik,* and Alfredo Caceres

Instituto "Mercedes y Martin Fereyra," Cordoba 5000, Argentina; and * Harvard Medical School and Center for Neurologic Diseases, Department of Medicine (Division of Neurology), Brigham and Women's Hospital, Boston, Massachusetts 02115

Abstract. The distribution of membrane-bound organelles was studied in cultured hippocampal neurons after antisense oligonucleotide suppression of the kinesin-heavy chain (KHC). We observed reduced 3,3'-dihexyloxacarbocyanine iodide (DiOC6(3)) fluorescent staining in neurites and growth cones. In astrocytes, KHC suppression results in the disappearance of the DiOC6(3)-positive reticular network from the cell periphery, and a parallel accumulation of label within the cell center. On the other hand, mitochondria microtubules and microfilaments display a distribution that closely resembles that observed in control cells. KHC suppression of neurons and astrocytes completely inhibited the Brefeldin A–induced spreading and tubulation of the Golgi-associated structure enriched in mannose-6-phosphate receptors. In addition, KHC suppression prevents the low pH-induced anterograde redistribution of late endocytic structures. Taken collectively, these observations suggest that in living neurons, kinesin mediates the anterograde transport of tubulovesicular structures originated in the central vacuolar system (e.g., the endoplasmic reticulum) and that the regulation of kinesin-membrane interactions may be of key importance for determining the intracellular distribution of selected organelles.

KINESIN is a mechanochemical enzyme that can translocate vesicles toward the plus end of microtubules in vitro (Vale et al., 1985*b*; Porter et al., 1987; Scholey et al., 1985); on the basis of the polarity of kinesin's movement and its presence in neural cells, it was originally suggested that kinesin may act as a motor for anterograde axonal transport (Vale et al., 1985*a*; Brady, 1985). In vitro, the ATPase activity of this enzyme is thought to be mechanochemically coupled to the generation of force. This force presumably provides the energy required to translocate microtubules in the gliding assay and to move vesicles along microtubules in several reconstituted systems.

The passage from the in vitro phenomena attributed to kinesin to a discrete cellular role has proven somewhat elusive. Attempts to understand the function of kinesin in neurons have focused on the motoric activity of the enzyme and implicated it in the translocation of membrane-bound organelles (Brady et al., 1990; Hirokawa et al., 1991). Although the particular classes of organelles translocated by kinesin are unknown, the suppression of kinesin heavy chain (KHC)[1] in cultured rat hippocampal pyramidal neurons using antisense oligonucleotides resulted in the retention of certain molecules within the cell body. GAP-43, synapsin I, and the amyloid precursor protein (Ferreira et al., 1992, 1993), proteins that are normally located at the tips of growing neurites, were confined to the cell body in antisense treated neurons. In *Drosophila* larval neurons, KHC mutations impaired axon potential propagation and neurotransmitter release at nerve terminals (Gho et al., 1992), but had no apparent effect on the concentration of synaptic vesicles at nerve terminals. Thus, in this cell system, kinesin may be active in the transport of vesicles containing ion channels, but it may not affect the accumulation of synaptic vesicles. On the other hand, a KHC-like protein, unc-104, is required for axonal transport of synaptic vesicles in *Caenorhabditis elegans* (Hall and Hedgecock, 1991).

An important step for a better understanding of kinesin function in vivo would be to establish its role in organizing membrane traffic within the central vacuolar system, which consists of the ER, Golgi apparatus, secretory vesicles, endosomes, and lysosomes (Klausner et al., 1992). Movement of proteins between these organelles occurs by the budding and fusion of transport vesicles; the transport vesicles carry not only their cargo, but also molecules that specify their destination (Pelham, 1991). The vesicular carriers are also likely to contain proteins that are attachment sites for microtubule motors, since many transport steps involve the microtubule-dependent movement of vesicles over relatively long intracellular distances. While microtubules are most obviously required for vesicle transport along nerve axons,

Address all correspondence to Kenneth S. Kosik, M.D., Center for Neurologic Diseases, Brigham and Women's Hospital, 221 Longwood Avenue, Boston, MA 02115. Phone: (617) 732-6460; fax: (617) 732-7787.

1. *Abbreviations used in this paper*: BFA, Brefeldin A; $DiOC_6$, dihexyloxacarbocyanine iodide; KHC, kinesin heavy chain; LY, Lucifer yellow dilithium salt; Man II, mannosidase II; MTSB, microtubule-stabilizing buffer; M6PR, mannose-6-phosphate receptor; NBD, *N*-(ε7 nitrobenz-2-oxa-1,3 diazol-4yl amino caproyl D-erythro-sphingosine).

they may also be required for routing newly synthesized proteins between the peripheral ER, Golgi, and plasma membrane. Microtubules may maintain the cytological positioning of spread ER tubules to the cell periphery and the accumulation of the Golgi in the centrosomal region of the cell (for a review see Pelham, 1991, and references within). The problem of how these diverse functions could be mediated by one or two motor proteins has been turned completely around by the cloning of a profusion of cDNAs with predicted sequences that place them in families with the classical motor proteins (for a review see Endow and Titus, 1992). While these observations suggest that there is no shortage of microtubule motors for these varied tasks, the role of kinesin or dynein, as well as of the new motors, in organizing membrane traffic and organelle distribution within the central vacuolar system remains to be established.

Here, we suppressed the expression of KHC in hippocampal pyramidal neurons and examined the intracellular distribution of the endoplasmic reticulum. We identified conditions capable of unmasking a latent interaction of kinesin with two additional cellular compartments. Brefeldin A–induced tubulation of a Golgi-associated compartment enriched in mannose 6-phosphate receptors was inhibited by KHC antisense oligonucleotides, and the pH-induced redistribution of late endosomes to the cell periphery was inhibited. Taken collectively, these results suggest that in cultured nerve cells, kinesin is involved in anterograde spreading of tubulovesicular structures originating in the central vacuolar system.

Materials and Methods

Tissue Culture Methodology

Dissociated hippocampal pyramidal cell cultures were prepared and maintained on polylysine-coated coverslips as described elsewhere (Ferreira et al., 1992, 1993). Glial cell cultures were prepared as described by Banker (1980). Three days after plating glial cell cultures were treated with 5×10^{-6} M arabinosylcytosine for 48 h to suppress additional proliferation, allowing cells to spread and flatten; cells were used after 7–10 d in culture. These cultures stained positively (>90% of cells) with an antibody to glial fibrillary acidic protein.

Antisense Oligonucleotides

KHC expression was inhibited with antisense oligonucleotides as described previously (Ferreira et al., 1992, 1993). The antisense oligonucleotide −11+14 rkin used in these experiments consists of the sequence GCC-GGGTCCGCCATCTTTCTGGCAG, and it is the inverse complement of the rat nucleotides −11+14. The oligonucleotides were synthesized on a synthesizer (380 B; Applied Biosystems, Inc., Foster City, CA), purified over a NAP5 column (Pharmacia LKB Biotechnology, Inc., Piscataway, NJ), ethanol precipitated, and taken up in medium. The administration of oligonucleotides was as follows: 2–4 h after plating, when the hippocampal cells were transferred to serum-free medium, the oligonucleotide was added at 50 μM. The medium was supplemented with 25 μM additional oligonucleotide every 12 h from the time of plating for either 24 or 48 h. A similar schedule was applied to 1-wk-old astrocyte cultures maintained in serum-free medium. Controls were treated with the same concentration and dosage schedule as the corresponding sense-strand oligonucleotide.

Dihexyloxacarbocyanine Iodide (DiOC6(3)) Staining of Cultures

Protocols for staining fixed cultures were essentially the same as reported by Terasaki et al. (1984). 2 ml of warm (37°C) fixative (0.25% glutaraldehyde in 0.1 M cacodylate buffer containing 5 mM calcium chloride) was added dropwise immediately after removal of the coverslips with the attached cells from the incubator. After 2–5 min, cultures were rinsed several times with fresh buffer. Fixed cultures were prepared for microscope examination as described by Dailey and Bridgman (1989). The coverslips were mounted with buffer on a glass microscope slide; two thin strips of No. 0 coverglass were used as spacers between the microscopic slide and the coverslip. Excess buffer was removed, and the chamber was sealed with hot wax. Slices were then placed on an inverted microscope (ICM 35M; Carl Zeiss, Inc., Thornwood, NY) equipped with Nomarski differential interference contrast, epifluorescence, and was observed with a 100× oil immersion objective. Photographs of neurons, neurites, and their growth cones were taken with a 35-mm camera attached to the inverted microscope using Kodak TMAX 400 ASA film; exposure times ranged from 45 to 60 s.

In some experiments, the relative intensity of DiOC6(3) staining was evaluated using quantitative fluorescence techniques as described by Keith (1991). To image labeled cells, the incoming epifluorescence illumination was attenuated with glass neural density filters. Images were recorded on the faceplate of a silicon-intensified target camera (SIT; Hamamatsu Corp., Middlesex, NJ) set for manual high voltage, gain, and black level. They were digitized directly into a video image processor (Jandel Video Analysis Software [JAVA]; Jandel Scientific, Corte Madeira, CA) controlled by a host IBM-AT computer. After digitization, images were corrected for shading distortion by dividing by a low pass–filtered image of a featureless field and normalizing to the maximum intensity within that image (flat field correction; Lim et al., 1990). Fluorescent intensity measurements were performed along the longitudinal axis of identified neurons using the line intensity menu of the JAVA set with a cursor window of 1×1 μm. Background levels were those detected in unlabeled cells.

Vital Staining the Golgi Apparatus

For staining the Golgi apparatus in living cells, astrocyte cultures were labeled with the sphingolipid C6-*N*-(ε7 nitrobenz-2-oxa-1,3 diazol-4yl amino caproyl D-erythro-sphingosine) (NBD)–ceramide (Lipsky and Pagano, 1985; Pagano et al., 1989), and were then examined by fluorescence microscopy. For these experiments, cells were grown in special petri dishes prepared according to the method of Dotti et al. (1988). Briefly, a 16-mm hole was drilled on the bottom of a petri dish (1006; Falcon Plastics, Cockeysville, MD), and a 22-mm glass coverslip was attached to the outer surface of the dish with a mixture or paraffin/petrolatum (3:1). The coverslips were then cleaned and treated as regular ones. A stock solution of 4 mM NBD-ceramide (Molecular Probes, Inc., Eugene, OR), made by dissolving the lipid in DMSO (Sigma Chemical Co., St. Louis, MO), was stored as 10-μl aliquots at 4°C in the dark. Aliquots of the fluorescent lipid were diluted to 40 μM in serum-free medium, and astrocyte cultures were labeled with this solution for 10 min. The cells were then washed twice with culture medium and incubated at 37°C for 30 or 60 min; immediately afterwards, the special petri dishes were placed on the heated stage of the inverted microscope. The cells were then observed using the 100× immersion objective for 1–120 min. Epifluorescence illumination was attenuated with neutral density filters, and images were formed with the silicon-intensified target camera as described. For purpose of presentation, fluorescent images were photographed directly off a high resolution video monitor (DAGE MTI, Michigan City, IN) using the automatic exposure setting of a 35-mm camera onto Kodak 100 ASA film (Eastman Kodak Co., Rochester, NY). The resulting negatives were then printed at the same exposure.

Rhodamine 123 Labeling of Mitochondria

For staining mitochondria in living neurons and astrocytes, cells were incubated with 10 μg/ml of rhodamine 123 diluted in serum-free medium for 5 min at 37°C. They were then observed and photographed as described for the cultures stained with NBD-ceramide.

Brefeldin A (BFA) Treatment of Nerve Cell Cultures

BFA was purchased from Epicentre Biotechnology (Madison, WI). Cells were treated with 10 μg/ml BFA for various periods of time, and at the end of each experiment, they were fixed and processed for immunofluorescence (see below).

Internalization of Endocytic Markers and Acidification

Lucifer yellow (LY dilithium salt; Sigma Chemical Co., St. Louis, MO) was inactivated as described by Bomsel et al. (1989) and was added at a concentration of 10 mg/ml to serum-free medium. Hippocampal cells were incubated with inactivated LY for ≤60 min, and were chased in marker free

medium for an additional 30 min to label late endocytic structures (Parton et al., 1991). The cells were then incubated for 15 min with Ringer's solution, pH 7.2 (155 mM NaCl, 5 mM KCl, 2 mM $CaCl_2$, 2 mM NaH_2PO_4, 10 mM Hepes, pH 7.2, 10 mM glucose, and 0.5% bovine serum albumin) or acetate Ringer's solution, pH 6.9 (the same as normal Ringer's solution with the following changes: 80 mM NaCl, 70 mM Na acetate, and 10 mM Hepes, pH 6.9), to analyze the distribution of late endosomes at normal pH and after intracellular acidification. After incubation in the appropriate buffer, the cells were fixed with cold methanol for 10 min. They were then observed in the microscope in a manner similar to that described for the DiOC6(3)-stained cultures. The relative intensity and distribution of LY was evaluated using quantitative fluorescent techniques as previously described. For these experiments, we use the line intensity menu of the JAVA, and measurements were performed pixel by pixel along the longitudinal axis of identified neurons.

Quantification of Kinesin and Microtubule Protein Levels

Whole cell homogenates and cytoskeletal fractions from cell cultures were prepared as described by Caceres et al. (1992), and the levels of KHC and tubulin were determined by dot immunobinding with iodinated protein A (Caceres et al., 1992; Ferreira et al., 1992). The following primary antibodies were used: a mouse mAb against bovine brain kinesin (clone IBII; Sigma Chemical Co.) and an mAb against total α-tubulin (clone DM1A; Sigma Chemical Co.).

Cytoskeletal Preparations and Fixation Protocols

For cytoskeletal preparations, the cells were rinsed once in microtubule-stabilizing buffer (MTSB): 100 mM 2-[*N*-morpholino]ethane sulfonic acid (MES) buffer adjusted with KOH to pH 6.8, 5 mM EGTA, 1 mM $MgCl_2$, and 20% glycerol) and then extracted with MTSB containing 0.2% Triton X-100 for 60 s (Caceres et al., 1992). For immunostaining, the cytoskeletons were rinsed carefully with MTSB without Triton, fixed in 3.5% paraformaldehyde-0.25% glutaraldehyde for 20 min, and then incubated sequentially in 0.15 M glycine buffered at pH 7.4 with Tris base, blocked in 1% bovine serum albumin in PBS, and stained by indirect immunofluorescence (see below). In other cases, cells were fixed for 10 min with cold methanol or for 30 min with warmed 4% paraformaldehyde in PBS containing 0.12 M sucrose as described elsewhere (Caceres et al., 1992).

Immunofluorescence

The antibody-staining protocol entailed labeling with the first primary, washing with PBS, 10 mg/ml bovine serum albumin, 0.1% Tween 20 (5× 2 min), labeling with second primary antibody, washing similarly, then staining with both labeled secondary antibodies. The primary antibodies used were a rabbit polyclonal antiserum against the chicken cation-independent mannose-6-phosphate receptor (a generous gift from Dr. B. Hoflack, EMBL, Heidelberg, Germany) diluted 1:50 or 1:150; an mAb against Golgi mannosidase II (mouse IgG, a generous gift of Brian Burke, Harvard Medical School, Boston, MA) diluted 1:5; and an mAb against α-tubulin (clone DM1A; Sigma Chemical Company) diluted 1:100 or 1:200. Secondary antibodies were goat anti-rabbit IgG rhodamine conjugated and goat anti-mouse IgG fluorescein conjugated (Boehringer Mannheim Biochemicals, Indianapolis, IN). Incubations with primary antibodies took place overnight at 4°C, while incubations with secondary antibodies were for 1 h at 37°C. In some experiments, fluorescein-labeled phalloidin (Molecular Probes, Inc.) was included with the secondary antibody to visualize filamentous actin. Coverslips were mounted with Fluorosave (Calbiochem-Novabiochem Corp., La Jolla, CA); cells were photographed using a 100× immersion objective on the inverted microscope using Kodak 400 ASA film.

Morphometric Analyses

Total neuritic length, the areas of growth cones and of the growth cones' DiOC6(3) mass were measured using the morphometric menu of the JAVA. Cells were observed using differential interference contrast optics of epifluorescence and were captured on the screen of the high resolution video monitor; a 2× zoom was applied to each image, and measurements were made directly from the video monitor screen.

Results

DiOC6(3) Staining of Kinesin-suppressed Hippocampal Nerve Cells

DiOC6(3) has been previously used to stain vesicle-like organelles and the plasma membrane in the nonneuronal cells (Terasaki et al., 1984) and peripheral neurons (Dailey and Bridgman, 1989). In these cells, labeled organelles have distinct intensities such that a reticular network appears intermediate between the faintly stained plasma membrane and the intensely fluorescent mitochondria. A body of evidence strongly suggests that the DiOC6(3)-stained reticular network is the ER (Terasaki et al., 1984; Dailey and Bridgman, 1989).

Hippocampal pyramidal neurons from control (nontreated) and sense-treated cultures display a pattern of DiOC6(3) staining that is similar to that described for cultured neurons of the rat superior cervical ganglion (Dailey and Bridgman, 1989). Thus, DiOC6(3)-stained hippocampal neurons show intense fluorescence throughout the cell bodies and neurites (Fig. 1 *a*). Mitochondria appeared as intensely fluorescent spots or elongated figures. The staining invariably extends into the base and central region of neuritic growth cones. In contrast, there was a considerable reduction of labeling in neurites and growth cones of cells treated with KHC antisense oligonucleotides; under this condition, intense staining was mainly confined to the cell body (Fig. 1 *b*).

The decrease in DiOC6(3) staining of kinesin suppressed neurons was best visualized in growth cones. In control cells, DiOC6(3) staining revealed a mass of labeling that filled the base and central region of growth cones (Fig. 1, *c* and *d*). Frequently, part of the DiOC6(3) mass extended into the peripheral regions of the growth cone. Another distinctive feature of the labeling was the presence of thin, moderately bright finger-like processes that radiated from the central mass into the growth cone margin (Fig. 1 *d*). Antisense-treated neurons showed a marked reduction in DiOC6(3) labeling in their growth cones (Fig. 1, *e* and *f*); it was not possible to observe any accumulation of labeling such as spots or finger-like processes. The most frequently detected elements in the growth cones of KHC-suppressed neurons after staining with DiOC6(3) were elongated bright figures resembling mitochondria that were usually located at the base and central region of growth cones. Measurements of fluorescence intensity confirmed our visual impression and revealed unambiguously the decrease in DiOC6(3) staining within neurites and growth cones of KHC-suppressed neurons (Fig. 2); this phenomenon was also observed after vital staining. A concomitant reduction in growth cone area accompanied this loss of DiOC6(3) labeling (Table I).

We next analyzed the pattern of DiOC6(3) staining in astrocytes to determine if kinesin suppression alters the distribution of this label similarly to the primary neurons. An additional advantage was that in flat cells, such as astrocytes, it is possible to stain the ER with DiOC6(3) as a moderately intense, polygonally shaped continuous array of thin tubules extending from the cell center into the peripheral regions of the cytoplasm. 1-wk-old astrocyte cultures were used for this experiment. The cells were treated with 50 μM KHC antisense oligonucleotides every 12 h for 2–3 d, then fixed and stained. Inhibition of kinesin expression was determined

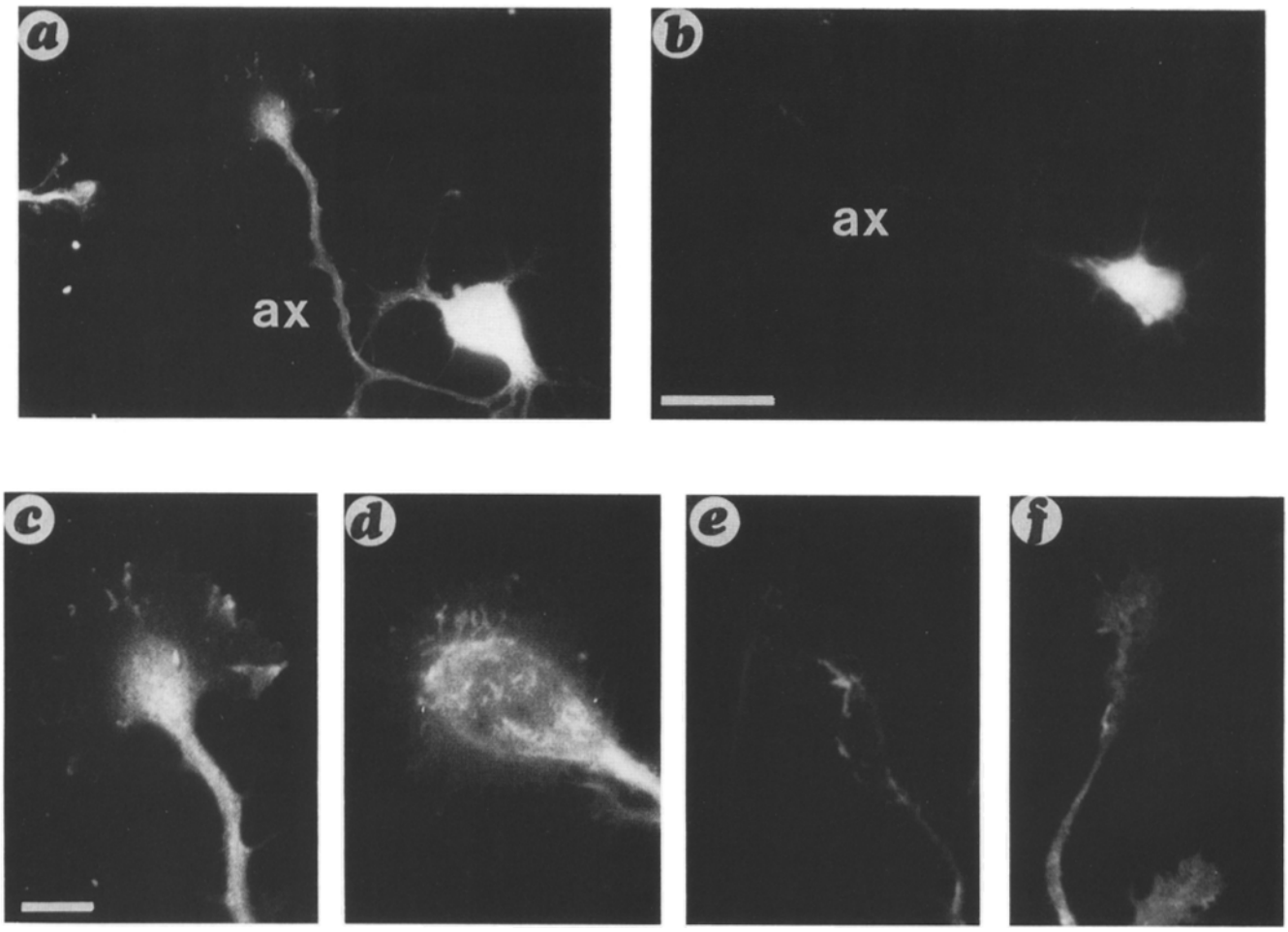

Figure 1. The distribution of DiOC6(3) staining in control nontreated (*a*) and KHC antisense-treated (*b*) hippocampal pyramidal neurons after development in culture for 1 d. In control cells, DiOC6(3) staining is uniformly distributed within the cell body and neurites. Note the decrease of labeling in the neurites of the antisense-treated neuron. (*c–f*) High power micrographs of growth cones from nontreated (*c*), sense-treated (*d*), and antisense-treated (*e* and *f*) neurons. In control cells, a mass of DiOC6(3) labeling occupies the central region of the growth cone with finger-like projections extending to the margin. In contrast, a considerable decrease of labeling is observed in the growth cones of antisense-treated neurons. Bars, 10 μm in *a* and *b*; 5 μm in *c–f*.

by immunofluorescence. KHC antisense–treated astrocytes showed only trace amounts of kinesin immunolabeling as opposed to control astrocytes, which displayed intense fluorescence. Dot immunobinding confirmed the decrease in KHC protein levels in the antisense treated cells (Table II). The DiOC6(3)-positive reticular network, which was easily detected in control astrocytes, completely disappeared in the cell periphery after antisense treatment, while an accumula-

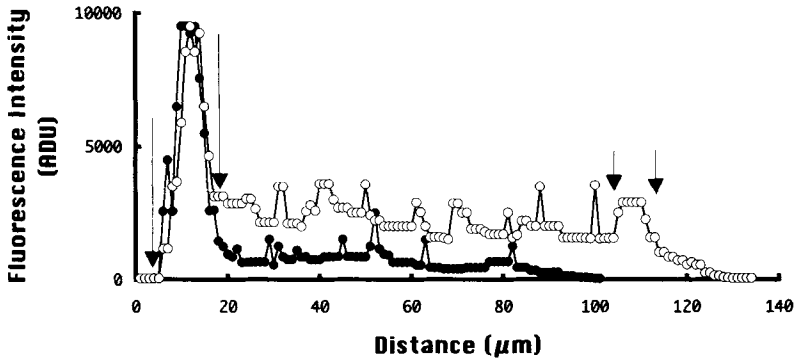

Figure 2. Graph showing the distribution of DiOC6(3) fluorescence intensity along the cell body and axon-like neurite of a control (*open circles*) and KHC antisense–treated (*solid circles*) hippocampal pyramidal neurons. All data are plotted along the longitudinal axis of the labeled neurons, starting at the cell body. Each point represents the fluorescent intensity measured in a 1 × 1-μm segment. The long arrows point to the beginning and end of the cell body, while the short ones indicate the central growth cone region of the control cell. Note the decrease of labeling in the antisense-treated neurons. The peaks of fluorescence intensity detected along neurites represent mitochondria and other discrete vesicle-like organelles. Measurements were performed in 25 cells for each experimental condition; the DiOC6(3) distribution profiles and the values of fluorescent intensities were similar to the ones displayed in the present graph. *ADU*, arbitrary analogue to digital units.

Table I. Neuronal Shape Parameters

	Total neuritic length	Growth cone area	Area DiOC6(3) growth cone mass
Control neurons	269 ± 12	320 ± 35	85 ± 5
Sense-treated neurons	245 ± 24	298 ± 12	78 ± 10
KHC antisense–treated neurons RK-11/14	160 ± 12	105 ± 10	15 ± 2

Each value represents the mean ± SEM. Area values are expressed in square micrometers and neurite length in micrometers. All measurements were performed in neurons that have been in culture for 1 d. A total of 50 cells and 150 growth cones were measured for each experimental group.

Table II. Quantification of Microtubule Protein Levels in Astrocytes

	Kinesin heavy chain	Total α-tubulin	Polymerized α-tubulin
Control cells	1350 ± 150	4500 ± 220	1300 ± 45
KHC antisense–treated astrocytes	220 ± 50	4350 ± 180	1260 ± 80

Microtubule protein levels wre determined by a dot immunobinding assay. Each value represents the mean ±SEM. Values are expressed in counts per minute per micrograms of total cellular protein. KHC and total α-tubulin protein levels were determined in samples obtained from whole-cell extracts while polymerized α-tubulin were determined in samples from cytoskeletal preparations. Five different cultures were used for each experimental condition. Background levels were 180 ± 20 cpm.

tion of label was observed in the immediate vicinity of the nucleus (Fig. 3). This phenomenon was not accompanied by changes in the microtubule distribution, as revealed by immunolabeling of cytoskeletal preparations with antibodies against α-tubulin. In antisense oligonucleotide–treated cells, microtubules radiated from the cell center into the peripheral cytoplasm with a pattern identical to that observed in control cells (Fig. 4).

Mitochondria were also present in areas devoid of reticular staining. To analyze the distribution of mitochondria in kinesin-suppressed neurons, living cultures were stained with rhodamine 123 (Fig. 5). In control cells, mitochondria were uniformly distributed throughout the whole extent of the cytoplasm; in the case of neurons, mitochondria were seen to extend up to the tip of growing neurites. This pattern was not altered by KHC suppression (Fig. 5). As observed by video microscopy, the typical pattern of mitochondrial movement, characterized by rapid anterograde and retrograde displacements, was unaffected in the KHC antisense oligonucleotide–treated cells.

BFA Treatment of KHC-suppressed Nerve Cells

BFA causes a microtubule-dependent redistribution of the Golgi complex into the ER, eliminating the Golgi apparatus as a morphologically distinct structure (Lippincott-Schwartz et al., 1989); markers of the *cis*-Golgi, such as the enzyme mannosidase II (Man II), or of the *trans*-Golgi, such as the lipid NBD-ceramide, were shown to redistribute into the ER (Klausner et al., 1992). This drug also induces a microtubule-dependent redistribution of a perinuclear compartment enriched in the mannose-6-phosphate receptor into extensive tubular processes (Wood et al., 1991; Damke et al., 1991).

Because BFA has both species-specific and cell type–specific effects, we first determined that BFA induced the redistribution of the Golgi membranes in neurons and astrocytes. In control neurons, Man II is restricted to the cell body, where it appears as a single, intensely bright immunofluorescent spot located in the immediate vicinity of the cell nucleus. In astrocytes, the Golgi apparatus, as revealed by immunostaining with the Man II antibody, ranges in appearance from small discrete elements to highly elongated tubulovesicular profiles that frequently form reticular networks interconnected over distances of ≤30–40 μm (Fig. 6, *a–c*). Similar morphologies were observed by vital staining of neurons and astrocytes with NBD-ceramide. BFA (10 μg/ml) treatment caused a rapid and dramatic change in the staining pattern observed with the markers of the Golgi apparatus in control and sense-treated astrocytes (Fig. 6, *d–i*). The disappearance of the Golgi cisternae as a defined structure was first detected 5 min after the addition of BFA (Fig. 6, *d* and *i*); when the cells were maintained in the presence of the drug for 10 or 15 min, the Golgi apparatus appeared as a fine punctate structure spread over the entire extent of the cytoplasm as detected with the Man II antibody (Fig. 6, *e* and *f*) or NBD-ceramide (Fig. 6, *h* and *i*).

The localization and morphology of the Golgi apparatus was significantly modified after KHC suppression. There was a significant reduction in the size, number, and spreading of labeled cisternae, a phenomenon that was accompanied by a collapse of the Golgi complex into the center of the cell (Fig. 7, *a–d*). BFA also induced a rapid redistribution of Golgi markers in cells treated with KHC antisense oligonucleotides. In these cells, the Golgi apparatus disappeared as a defined organelle, and diffuse labeling was observed around the nucleus and in the central region of the cytoplasm. The time course of the BFA-induced redistribution of the Golgi apparatus in KHC-suppressed astrocytes was identical to that observed in control cells (Fig. 7, *e–g*). A similar phenomenon occurred in neurons (data not shown).

We next analyzed the fate of mannose-6-phosphate receptor (M6PR) immunolabeling after BFA treatment. Most of the M6PR is located in a functionally distinct specialized compartment close to the *trans*-Golgi network (Griffiths et al., 1988; Klumperman et al., 1993). In control neurons (nontreated or sense-treated), M6PR was restricted to the cell body, where it appears as a single bright immunofluorescent spot (Fig. 8 *a*) or a band that resembled a half moon. In most cases, the labeling was detected close to the nucleus; a similar pattern was observed in cells treated with KHC antisense oligonucleotides. M6PR redistribution was first detected 5 min after the addition of BFA in both nontreated and sense-treated neurons, and by 15 min, the labeling reached the cell periphery, including neurites and their growth cones (Fig. 8, *c–f*). The pattern of labeling closely follows the intracellular distribution of microtubules, a phenomenon particularly evident within growth cones. In this region, it was possible to observe tubular profiles enriched in M6PR codistributing with microtubules (Fig. 8, *e* and *f*). These profiles were detected ≤12 h after BFA treatment (the longest time period analyzed).

KHC antisense treatment completely blocked the BFA-induced redistribution of M6PR-enriched organelles (Fig. 8, *g* and *h*). Under these conditions, M6PR immunolabeling was confined to the cell body in an identical pattern to that

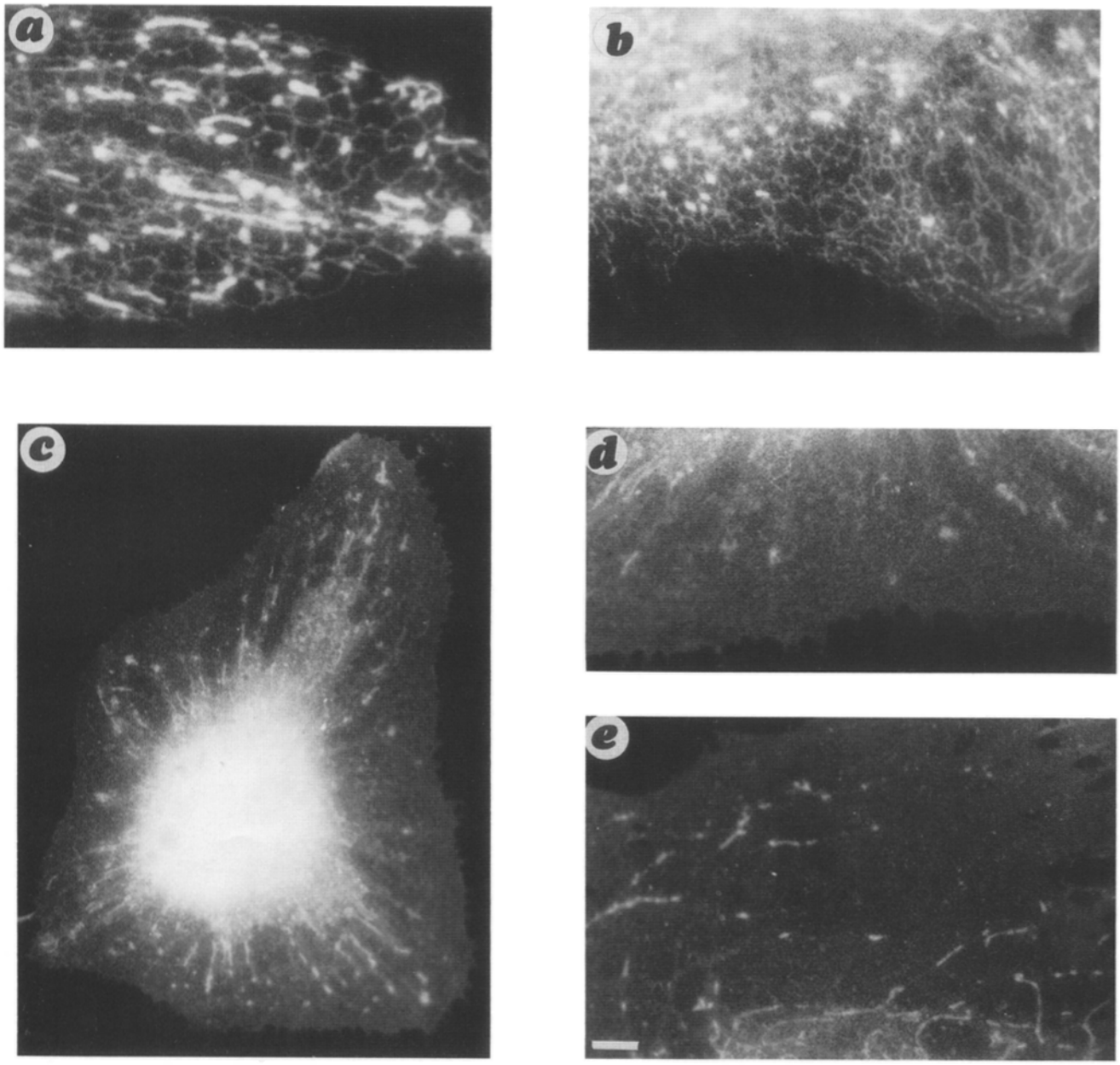

Figure 3. Micrographs showing the pattern of DiOC6(3) staining in nontreated (*a*), sense-treated (*b*), and KHC antisense–treated (*c*, *d*, and *e*) astrocytes. *a* and *b* show the labeling of the ER and other vesicle-like organelles in the peripheral cytoplasm of control cells. (*c*) Low power micrograph showing the distribution of DiOC6(3)-positive organelles in an antisense-treated astrocyte. An intense mass of labeling is detected at the center of the cell; vesicle-like organelles are observed throughout the cell cytoplasm. (*d*) High power micrograph of a region of the peripheral cytoplasm of the cell shown in *c*; note the absence of reticular staining at the cell periphery and the presence of elongated figures resembling mitochondria. (*e*) The cell margin of an antisense-treated astrocyte showing the disappearance of the DiOC6(3) ER labeling. Bar, 10 μm in *a*, *b*, *d*, and *e*; 5 μm in *c*.

observed in controls, as well as in cells treated with antisense oligonucleotides alone. In astrocytes, BFA also causes the rapid redistribution of M6PR immunolabeling throughout the cell cytoplasm; M6PR-enriched tubular profiles were associated with microtubules extending from the cell center to the peripheral cytoplasm (Fig. 9). As in the case of neurons, the BFA-induced redistribution of M6PR labeling was highly dependent on KHC expression (Fig. 10).

Figure 4. Micrographs showing the distribution of microtubules (*a* and *b*) and actin filaments (*c* and *d*) in control (*a* and *c*) and KHC antisense–treated (*b* and *d*) astrocytes. Under both conditions microtubules and microfilaments extend throughout the cell cytoplasm. Microtubules were labeled with an antibody against tyrosinated α-tubulin, and actin filaments were labeled with fluorescein-phalloidin. Bar, 10 μm.

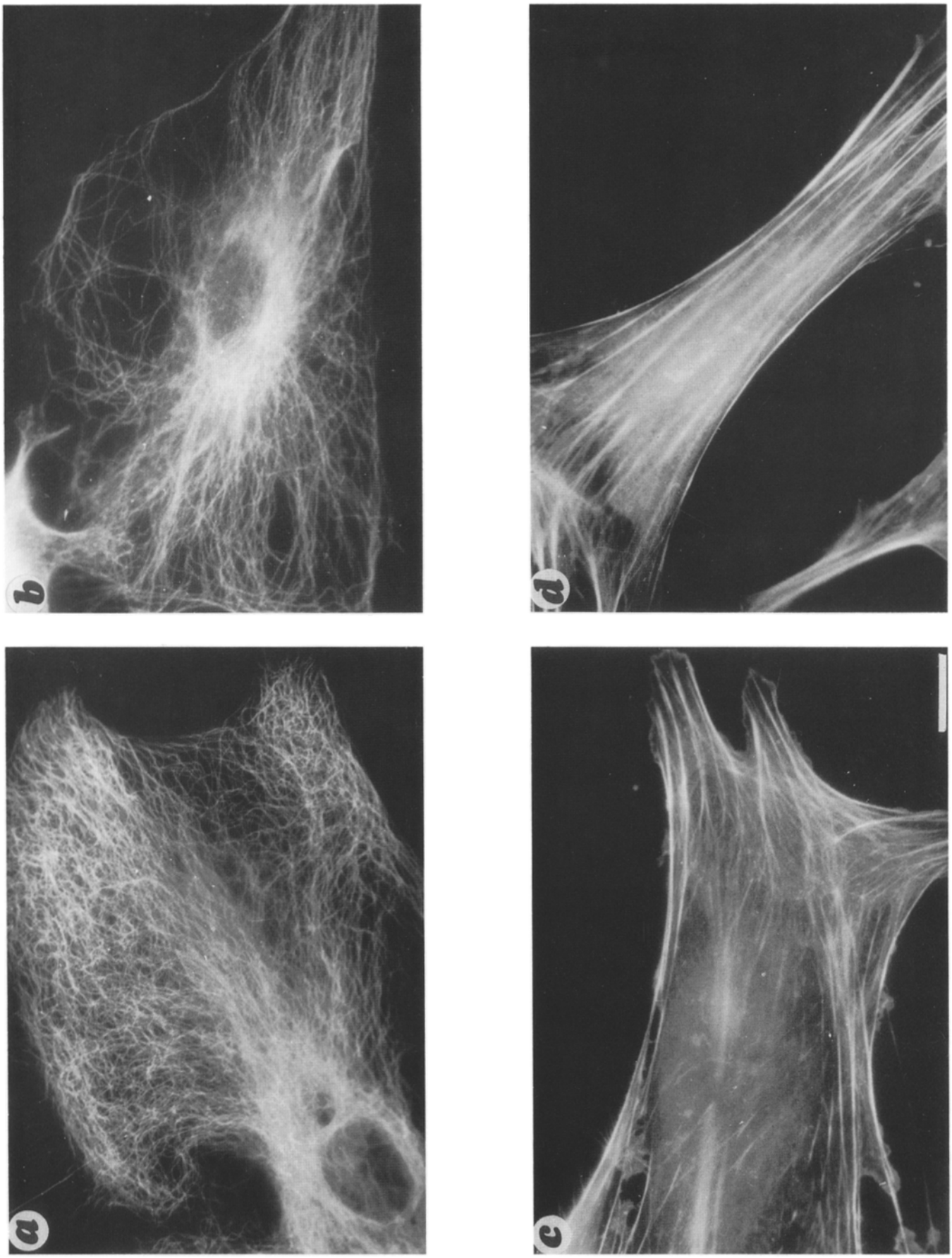
b
d
a
c

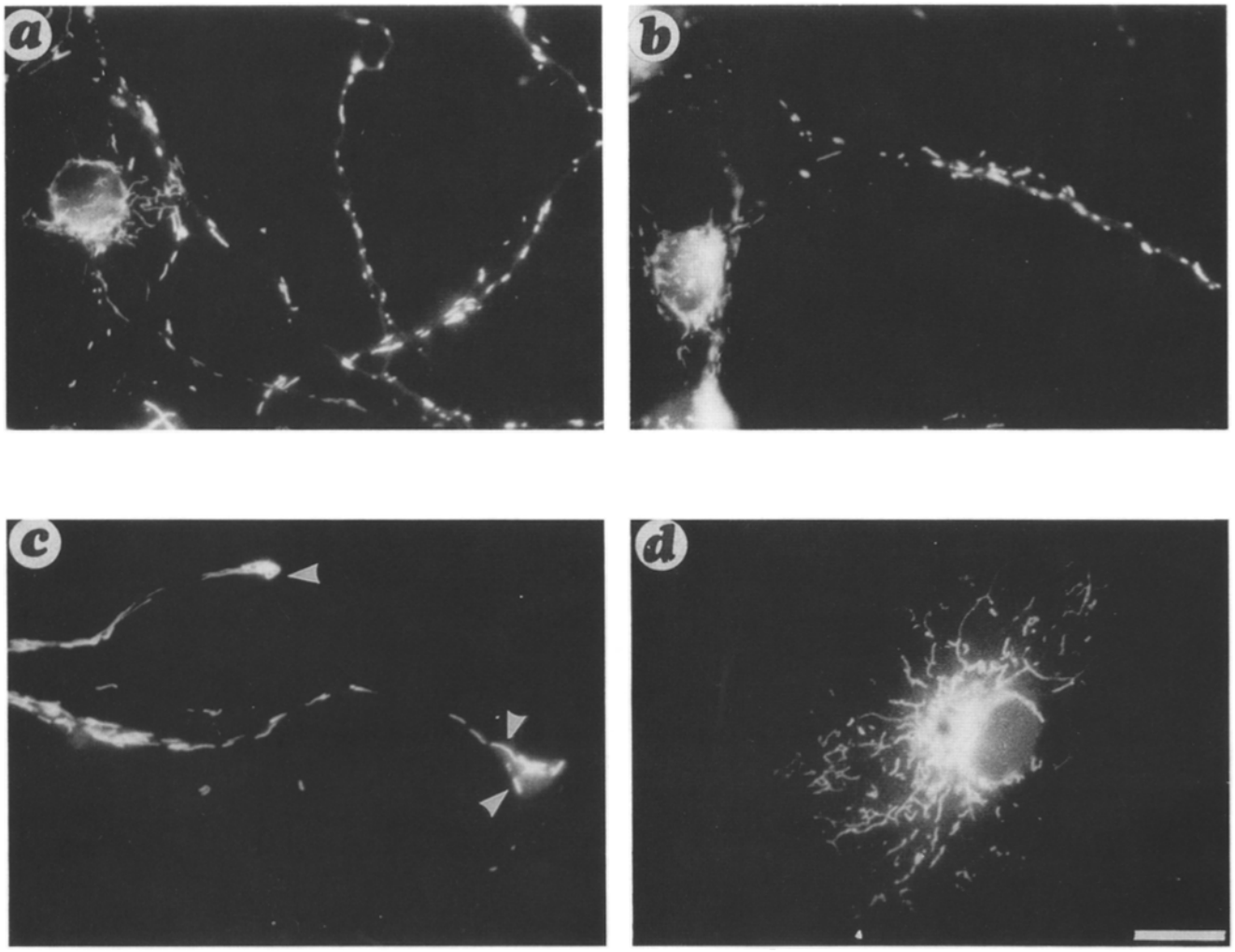

Figure 5. The distribution of mitochondria in sense-treated (*a*) and KHC antisense–treated (*b* and *c*) neurons as revealed by labeling of living cultures with rhodamine 123. In both cases, mitochondria are present in the cell body and neuritic processes. Note that in antisense-treated neurons, rhodamine 123 labeling is detected not only in proximal neuritic segments (*b*), but also at their tips (*c*, *arrowheads*). (*d*) Rhodamine 123 labeling of a KHC antisense–treated astrocytes. Note that mitochondria are distributed throughout the cell cytoplasm. Bar, 10 μm.

It remained possible that tubules formed, but they could not be detected with the M6PR marker. Therefore, BFA-treated cells were incubated for 5 min in LY to label retrogradely moving organelles. As described above, control astrocytes (nontreated or sense-treated) or KHC-suppressed cells incubated with LY for 5 min results in the labeling of small endosomal vesicles that are distributed throughout the cell periphery (Fig. 11). However, if astrocytes from control cultures were pretreated with BFA for 10 min and then pulsed with LY for 5 min while still in BFA, the fluid-phase marker now enters extensive tubular processes that radiate from the cell center to the peripheral cytoplasm (Fig. 11, *c* and *e*). These LY-labeled tubular profiles colocalized with the M6PR antibody. After a chase in marker-free medium, LY accumulated within the cell body, while M6PR labeling remained distributed throughout the cell cytoplasm. In contrast, no evidence of tubule formation was detected in the KHC antisense–treated astrocytes (Fig. 11, *d* and *f*); under this condition, LY was found in discrete punctate structures that remained distributed throughout the entire extent of the cytoplasm. Taken together, these results suggest that KHC suppression results in the inhibition of BFA-induced tubulation.

Internalization of Endocytic Markers and Low pH–induced Redistribution of Late Endosomes in KHC-suppressed Nerve Cells

To study the distribution and time course of internalization of the fluid-phase marker LY in cultured hippocampal pyramidal neurons, 1 d after plating, cells were incubated with LY, and fixed at 5-min intervals during a 40-min period. Some cultures were chased in marker-free medium for an additional 30 min. Internalized LY was visualized as punctate labeling in the cell body, neurites, and growth cones within 5 min after incubation in marker-containing medium, and labeling was maximum after a 30-min incubation. The site of greatest internalization was the cell body followed by growth cones and neurites. When chased in marker-free medium, there was a progressive accumulation of labeling

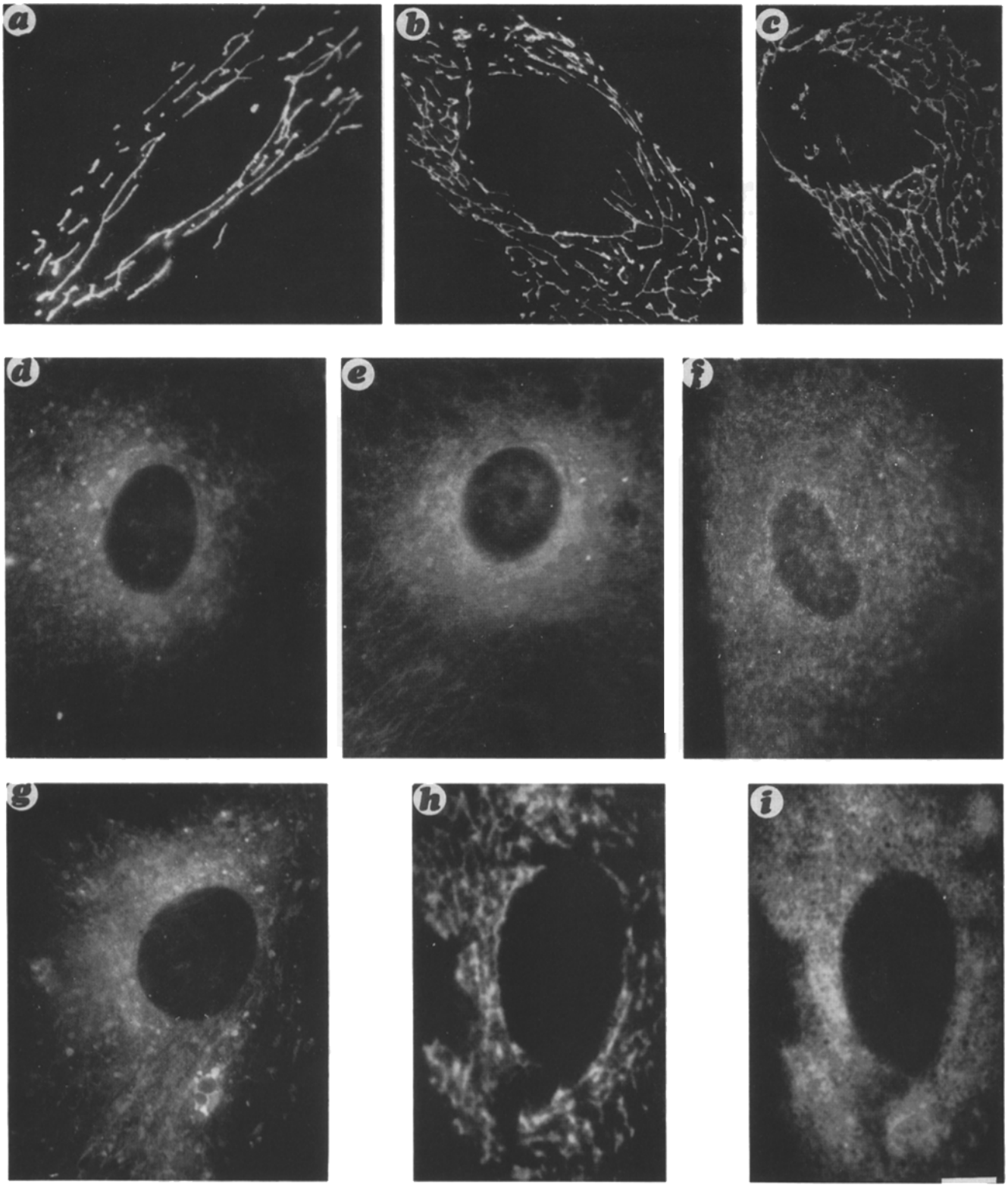

Figure 6. (*a–c*) Fluorescent micrographs showing the morphology of the Golgi apparatus in nontreated (*a*) and sense-treated (*b* and *c*) astrocytes, as revealed by immunolabeling with a mAb against Man II. The Golgi apparatus appears as a reticulum of anastomosing branches located in the perinuclear region; tubulovesicular processes extend for considerable distances and frequently interconnect adjacent Golgi elements. (*d–f*) Micrographs showing the distribution of Man II after treatment of control astrocytes with BFA for 5 (*d*), 10 (*e*), or 15 (*f*) min. Note the disappearance of the Golgi complex as a compact structure; instead, punctate diffuse labeling is observed throughout the cytoplasm. (*g*) The disappearance of the Golgi complex in a sense oligonucleotide–treated astrocyte incubated with BFA for 10 min and stained with Man II. (*h* and *i*) The distribution of the Golgi complex in a living control astrocyte after labeling with the fluorescent lipid NBD-ceramide (*h*) and the same cell after 5 min in BFA (*i*). Note the disappearance of the Golgi complex. Bar, 10 μm.

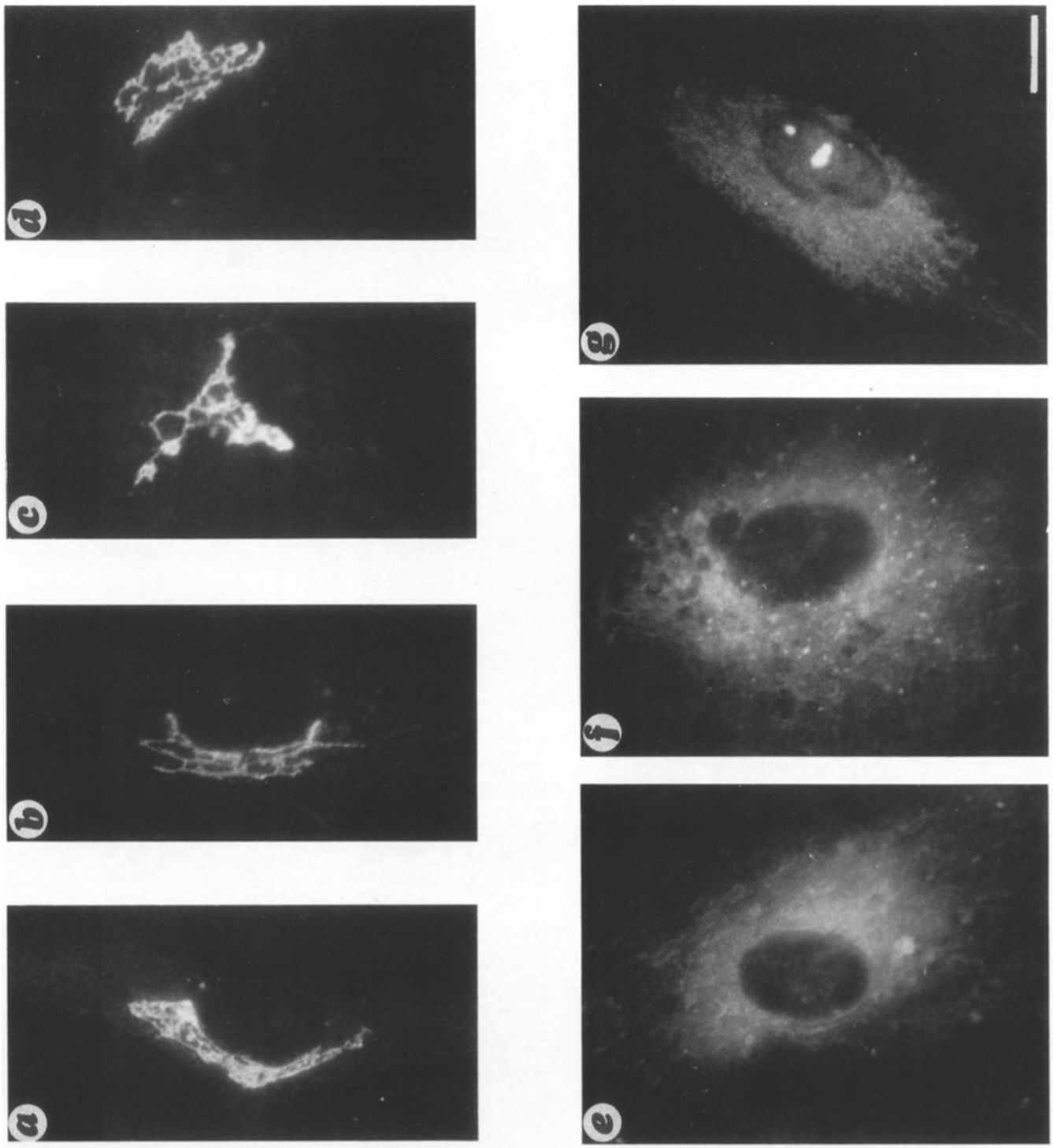

Figure 7. (*a–d*) Micrographs showing the morphology of the Golgi apparatus after KHC antisense oligonucleotide treatment in cells stained with the Man II antibody. Note the reduction in the size and number of labeled cisternae. The Golgi apparati have collapsed into the center of the cells. (*e–g*) Micrographs showing the distribution of Man II in KHC antisense-treated astrocytes after 5 (*e*), 10 (*f*), and 15 (*g*) min in the presence of BFA. Note the disappearance of the Golgi complex. Bar, 10 μm.

Figure 8. Double immunofluorescence micrographs showing the distribution of M6PR (*a*, *c*, *e*, and *g*) and α-tubulin (*b*, *d*, *f*, and *h*) in hippocampal pyramidal neurons after 1 d in culture. In control neurons (*a*), M6PR immunolabeling is detected as an intensely fluorescent spot located in the immediate vicinity of the cell nucleus (*arrowheads*). After a 5- (*c*) or 15-min (*e*) treatment with BFA, M6PR immunolabeling redistributes throughout the cell body and neurites including their growth cones (*gc* in *e*). Note the colocalization of M6PR-labeled tubular profiles with microtubules in neurites and the growth cone area (*f*). (*g* and *h*) KHC antisense treatment completely prevents the BFA-induced redistribution of the M6PR immunolabeling. Under this condition, staining is detected as a single fluorescent spot (*arrowhead*) located in close apposition to the cell nucleus. Bar, 10 μm.

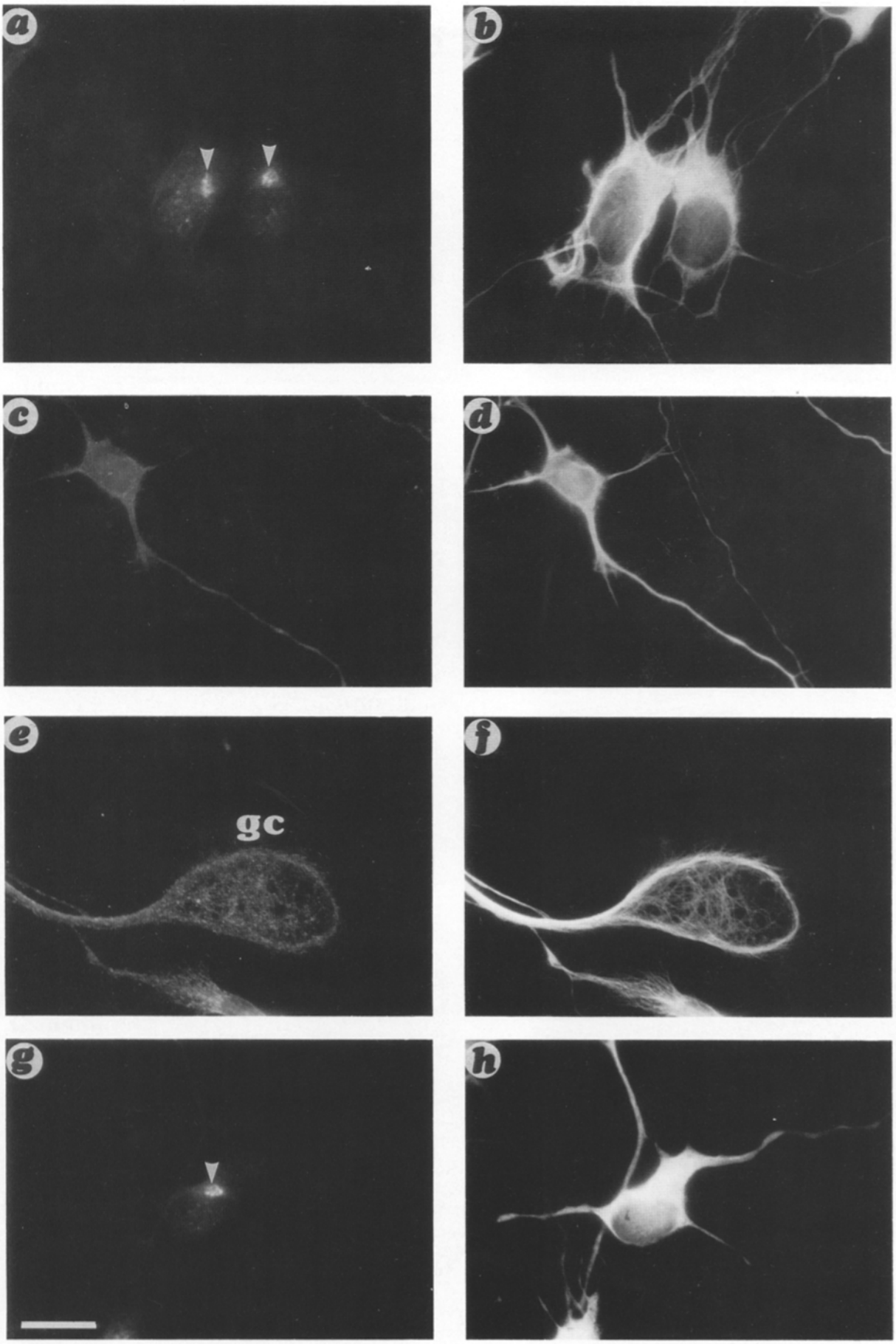
a
b
c
d
e
gc
f
g
h

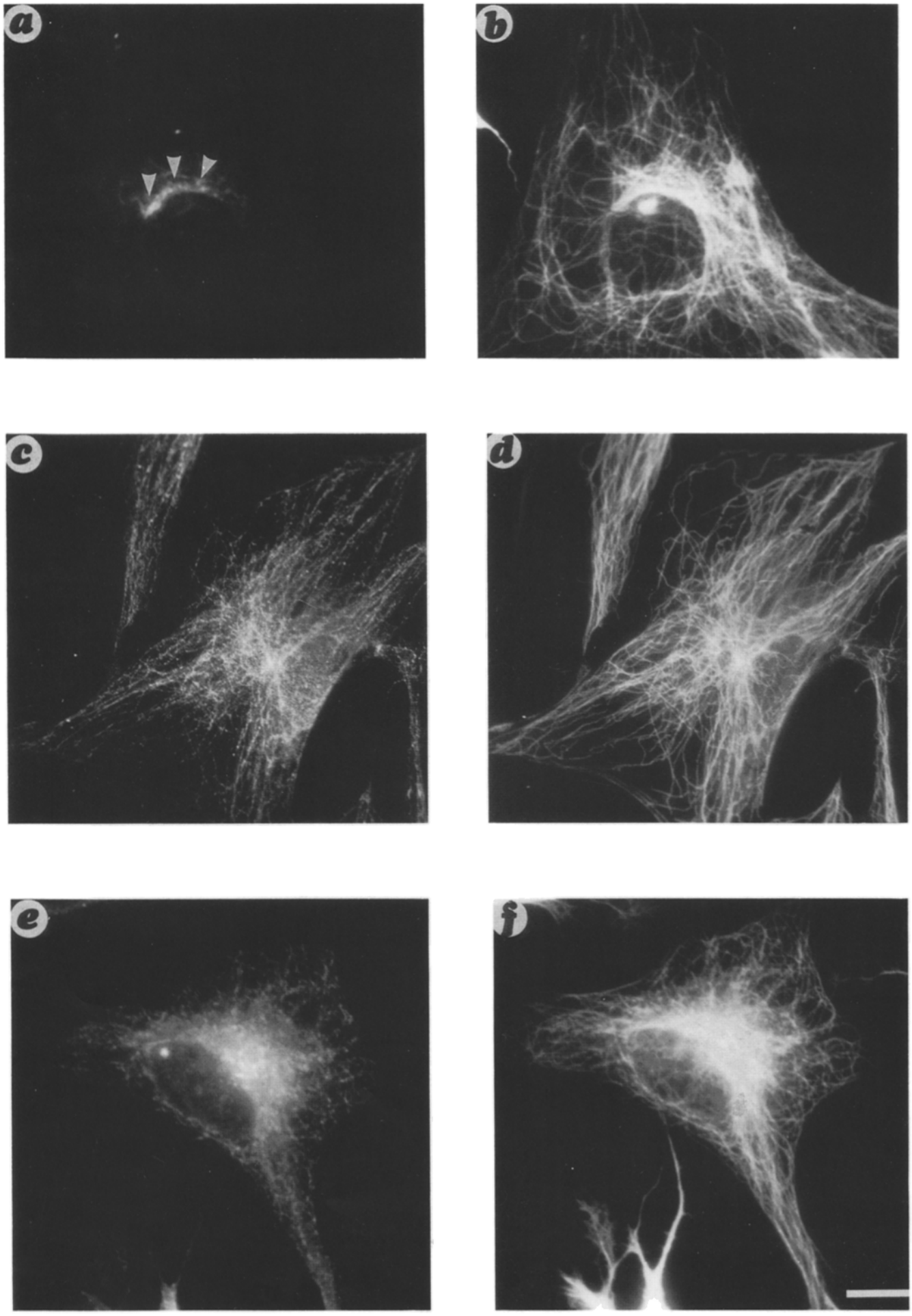
a
b
c
d
e
f

in proximal neuritic segments and in the cell body; by 30 min after the chase, LY was found almost exclusively in the cell body (Fig. 12). A similar pattern was observed in KHC antisense oligonucleotide–treated neurons.

Having observed that internalization of LY and its accumulation in the cell body were not modified by the presence of KHC antisense oligonucleotides, we lowered the pH to induce a redistribution of the labeled organelles. As previously reported by Parton et al. (1991), control cells kept in Ringer's solution, pH 7.2, after the chase period contained LY almost exclusively in the cell body, while in neurons incubated in acetate Ringer's solution, pH 6.9, punctate LY staining was detected in neuritic processes and their growth cones (Figs. 12 and 13). In contrast, KHC antisense oligonucleotide–treated neurons incubated with acetate Ringer's solution, pH 6.9, did not redistribute LY from the cell body to the neurites; instead, labeling remained in the cell body (Figs. 12 and 13).

Discussion

Kinesin and the Spreading of the Endoplasmic Reticulum

The observations presented here suggest that kinesin is involved in the anterograde spreading of tubulovesicular membranes originating in the central vacuolar system. The ER normally distributes to the cell periphery of astrocytes; in neurons, it extends along the processes to growth cones. In astrocytes, the loss of the ER from the cell periphery and the decrement of DiOC6(3) staining in neuritic processes suggests that an anterograde force generator is actively required to maintain this normal distribution.

Previous studies have shown that a tubulovesicular network analogous to the ER can form in vitro from membrane aggregates in the presence of microtubules and ATP; the sensitivity of network formation to adenylylimidodiphosphate, vanadate, and *N*-methylmaleimide suggested that ER spreading depended on the activity of a plus-end microtubule-based motor (Dabora and Sheetz, 1988; Vale and Hotani, 1988). The isolation of a 160-kD polypeptide from chicken brain microsomal fractions, termed kinectin, which is a major kinesin-binding protein on the ER (Toyoshima et al., 1992), gives further support to the idea that an important function of kinesin in living cells is to drive the anterograde transport of the ER. In this regard, it is worth noting that fluorescence microscopy has shown that KHC preferentially distributes along the ER (Hollenbeck, 1989; Brady and Pfister, 1991; Henson et al., 1992), just as the 160-kD protein does (Toyoshima et al., 1992).

Two models have been proposed to explain how microtubule-based motility generates the anterograde spreading of the ER (Dabora and Sheetz, 1989): in one model, a microtubule motor such as kinesin attaches to a region of a membrane aggregate and moves along a stationary microtubule pulling out a tubule, a phenomenon termed microtubule-dependent tethering; the alternative mechanism for producing the network is for membrane-attached microtubules to spread out tubulovesicular processes by microtubule sliding mediated by motors (see also Navone et al., 1992). Although it is presently difficult to distinguish between these possibilities, the fact that under our experimental conditions, we did not detect a decrease in microtubule polymer mass or modifications in the distribution of microtubules after antisense oligonucleotide treatment suggests that microtubule movement is not significantly altered after KHC suppression, and hence, may not be a primary determinant of the anterograde transport of the ER. It is also unlikely that the retraction of the ER observed in KHC-suppressed nerve cells is the consequence of actin depolymerization, since no differences in phalloidin staining were detected between control and the antisense oligonucleotide–treated cells. Instead, these results are more consistent with the idea that ER tubules are transported by kinesin molecules moving along microtubules.

Inhibition of BFA-induced Tubulation

The formation of tubulovesicular processes and the fusion of contracting membranes into a reticular network is not unique to the ER. Tubulovesicular elements emerging from the *trans*-Golgi and adjacent cisternae have been observed in living astrocytes labeled with NBD-ceramide. Similar to the morphogenesis of the ER, the spreading of reticular Golgi elements requires intact microtubules (Cooper et al., 1990). Because the Golgi complex collapsed after KHC suppression, its maintenance may require an anterograde motor. This requirement is likely to be indirect because kinesin has not been detected on Golgi membranes (Leopold et al., 1992; Fath et al., 1994), and it may involve a loss of plus-end constitutive recycling of Golgi components back to the ER. The extent of tubulation of the Golgi complex and the *trans*-Golgi network can be greatly enhanced by the drug BFA (for reviews see Klausner et al., 1992; Pelham, 1991). Upon treatment with BFA, the Golgi elements break down into numerous tubular profiles that move along microtubules carrying membranes into the ER (Lippincott-Schwartz et al., 1989, 1990). Tubule formation requires energy and can be inhibited at temperatures below 16°C by disruption of microtubules (Donaldson et al., 1991). The elongation rate of these tubular processes is >1–2 mm/min, suggesting a requirement for microtubule-based motors in their transport. Likewise in neurons and astrocytes, BFA also induced a dramatic redistribution of Golgi markers. Interestingly, both of these BFA-induced membrane processes extend from the cell center to the periphery, implying movement to the plus end of microtubules.

In neurons, KHC suppression by antisense oligonucleotide treatment completely prevented the BFA-induced redistribution of the M6PR-enriched compartment. This Golgi-associated structure (Griffiths et al., 1988), as detected with

Figure 9. Double immunofluorescence micrographs showing the distribution of M6PR (*a*, *c*, and *e*) and microtubules (*b*, *d*, and *f*) in astrocytes. M6PR immunolabeling is located in the perinuclear region (*arrowheads*). A 5- (*c*) or 15-min (*e*) treatment of these cells with BFA induced a dramatic redistribution of the labeling in which tubular profiles run in close apposition to the microtubules of the central and peripheral cytoplasm (*d* and *f*). Bar, 10 μm.

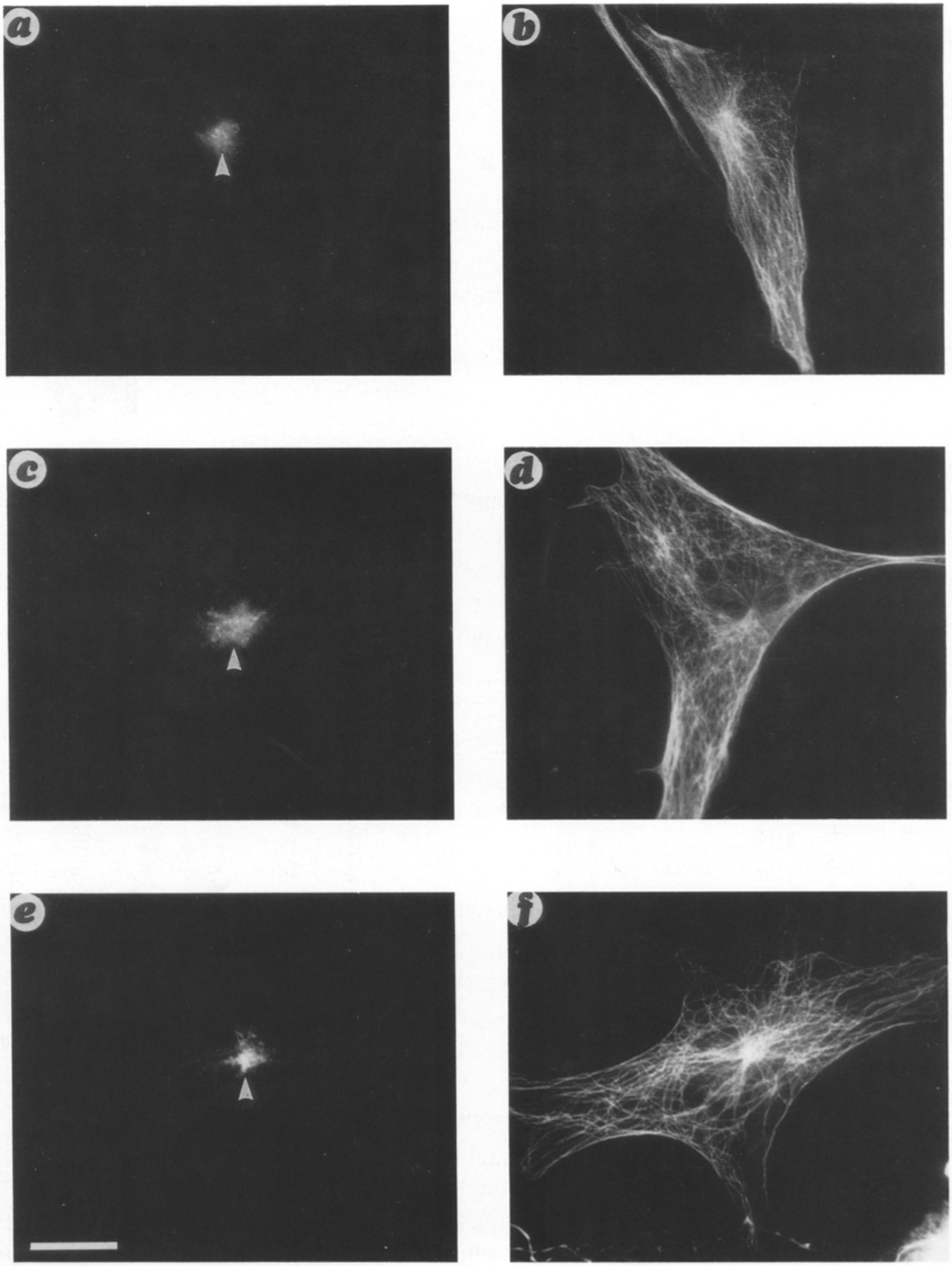

Figure 10. Double immunofluorescence micrographs showing the distribution of M6PR immunolabeling (*a*, *c*, and *e*) and microtubules (*b*, *d*, and *f*) in KHC-suppressed astrocytes treated with BFA for 5 (*a*), 10 (*c*), and 15 (*e*) min. As is the case of the neurons, KHC antisense oligonucleotide treatment completely blocks the BFA-induced redistribution of the M6PR immunolabeling. Note that the labeling remains localized to the center of the cell close to the nucleus. Bar, 10 μm.

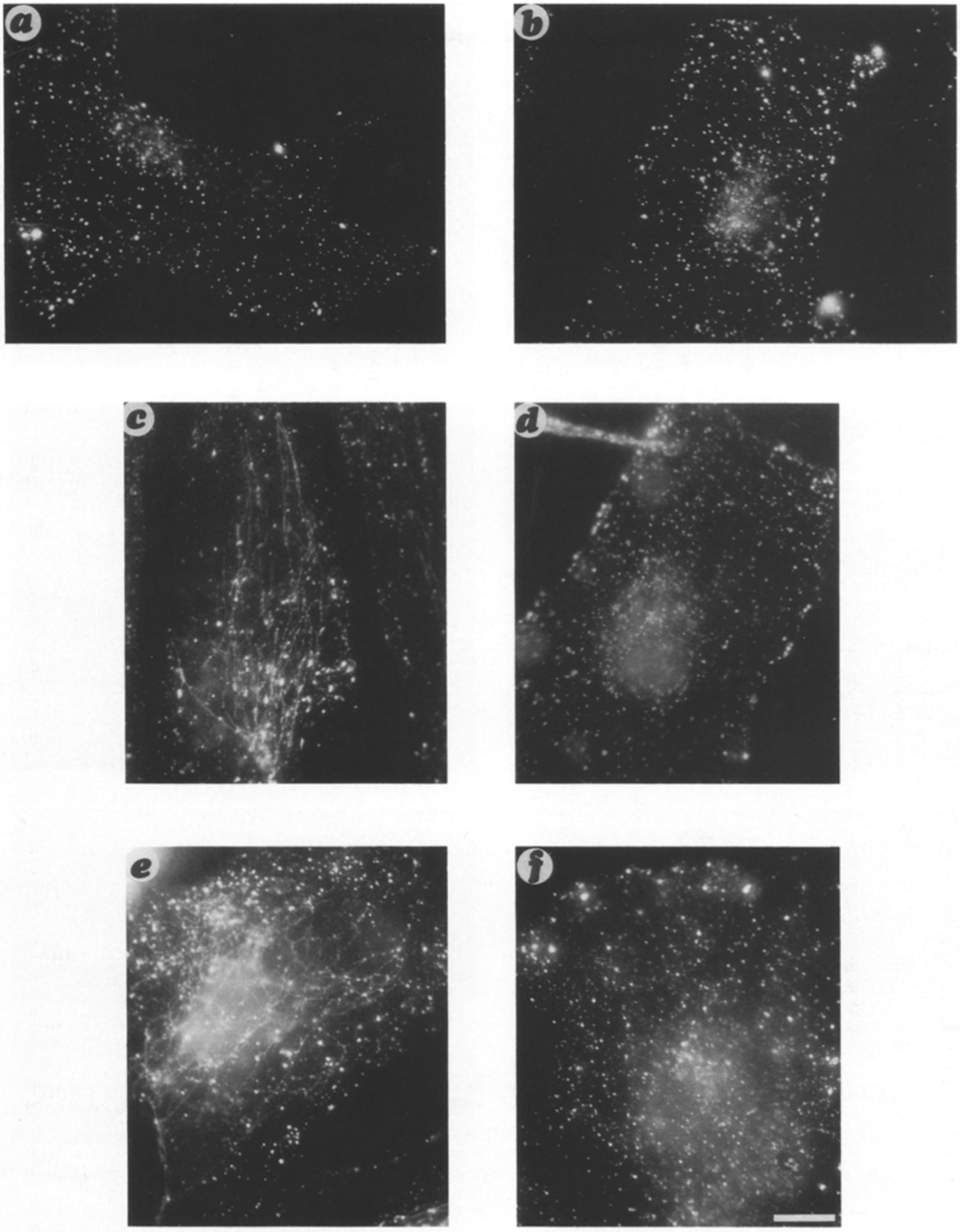

Figure 11. (*a* and *b*) Fluorescence micrographs showing the distribution of internalized LY (5 min pulse) in control (*a*) and KHC-suppressed (*b*) astrocytes. Under both conditions, a fine discrete punctate labeling appears throughout the cytoplasm. (*c* and *e*) Fluorescence micrographs showing the distribution of internalized LY (5-min pulse) in sense KHC oligonucleotide–treated astrocytes incubated for 10 (*c*) or 15 (*e*) min with BFA. Under this condition, the internalized fluid-phase marker distributes along tubular processes that extend from the cell center throughout the peripheral cytoplasm. In contrast, no evidence of tubule formation can be detected when KHC-suppressed astrocytes are pulsed for 5 min with LY while still in BFA for 10 (*d*) or 15 min (*f*). Bar, 10 μm.

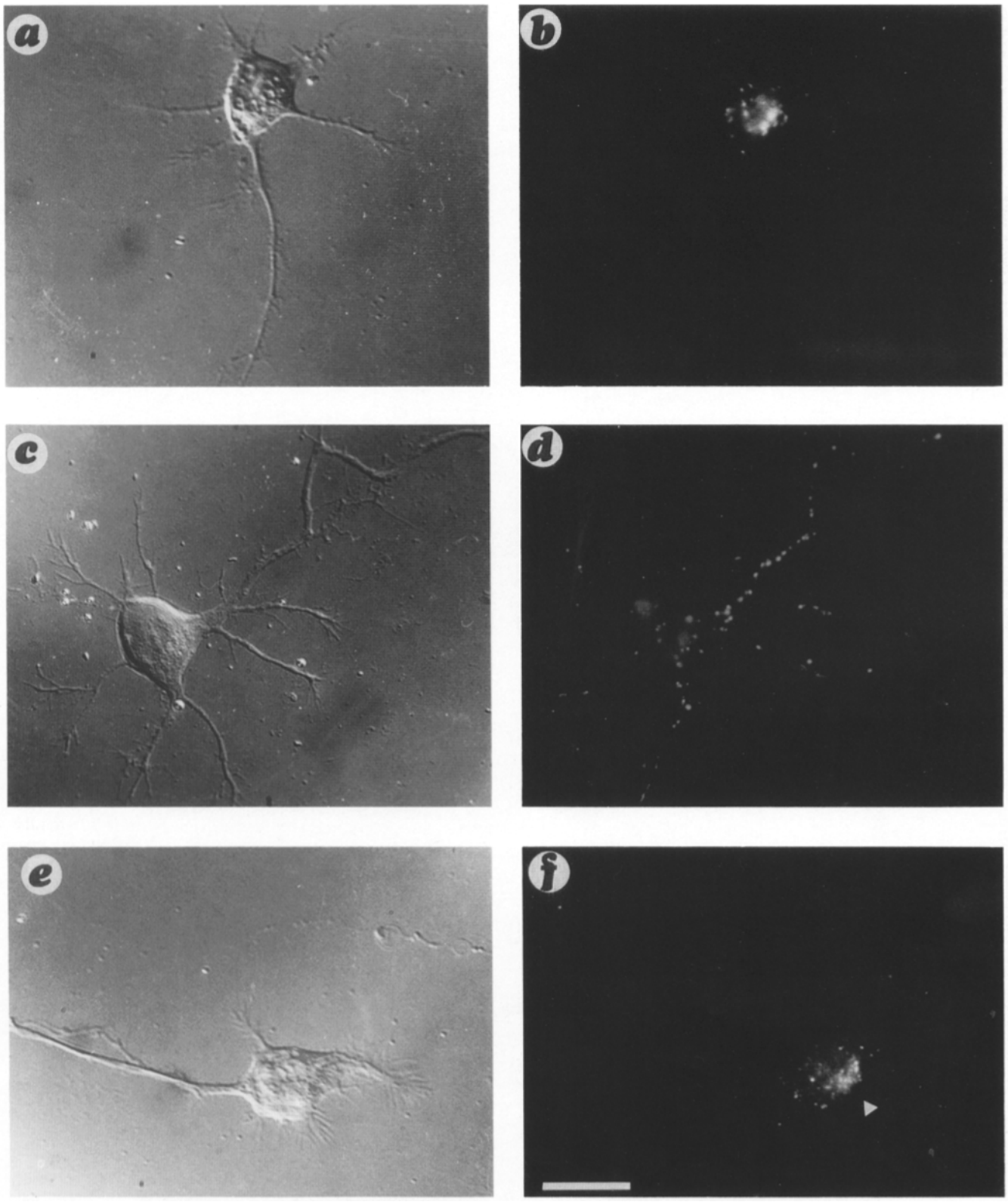

Figure 12. KHC suppression prevents the low pH-induced anterograde redistribution of late endosomes in hippocampal pyramidal neurons. After 1 d in culture, sense oligonucleotide-treated neurons were incubated for 40 min in LY-containing medium, chased for 30 min in marker-free medium, and further incubated for 15 min in Ringer's solution, pH 7.2 (*a* and *b*), or acetate Ringer's solution, pH 6.9 (*c* and *d*). At pH 7.2, virtually all the marker is concentrated in the cell body, while after incubation at pH 6.9, labeling is seen along the neurites, including their growth cones. In contrast, low pH does not induce an anterograde redistribution of LY-labeled late endocytic structures in KHC antisense oligonucleotide-treated neurons (*e* and *f*). Instead, the labeling remains localized at the cell body (*arrowhead*). Bar, 10 μm.

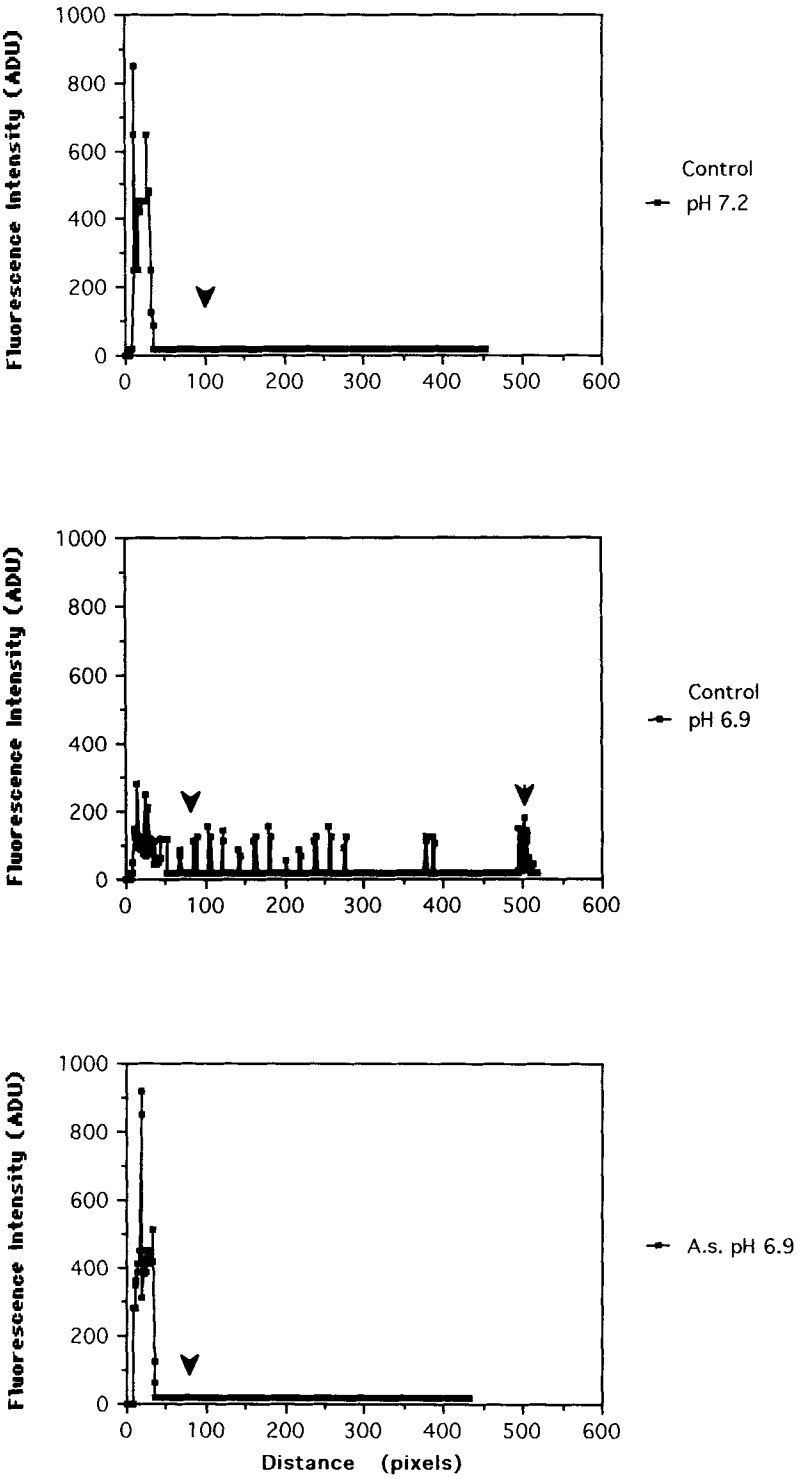

Figure 13. Graph showing the distribution of LY fluorescence intensity along the cell body and neurites of hippocampal pyramidal neurons incubated with the fluid-phase marker for 30 min, then chased in marker-free medium, and further incubated for 15 min with Ringer's solution, pH 7.2, or acetate Ringer's solution, pH 6.9. Data are plotted along the longitudinal axis of the labeled neurons starting at the cell body. The arrowheads indicate the end of the cell body. Each point represents the fluorescence intensity measured in a single pixel. In control neurons maintained at pH 7.2 after the chase period (control, pH 7.2), the labeling is concentrated in a discrete zone of the cell body, while in cells maintained at pH 6.9 (control, pH 6.9), the labeling redistributes towards the neurites including their growth cones (*small arrow*). In contrast, when KHC-suppressed neurons are maintained at pH 6.9 (antisense-treated, pH 6.9), the LY fluorescence fails to redistribute to the neurites and remains localized to the cell body. Measurements were performed in 30 cells for each experimental condition. The LY distribution profiles and the values of fluorescence intensities were similar to those displayed in the present graph. *ADU*, arbitrary analogue to digital units.

an antibody against the cation-independent M6PR, appeared as a single immunofluorescent spot located in the immediate vicinity of the cell nucleus. A complete blockade of the anterograde spreading of the M6PR immunolabeling was also detected in BFA-treated astrocytes in which KHC was suppressed. These results suggest that kinesin is involved in the anterograde transport of tubular profiles derived from this M6PR-enriched compartment; therefore, one consequence of BFA action involves an enhanced plus-end-directed motor activity rather than a release of Golgi elements from inhibition of minus-end-directed motors (Wood et al., 1991; Pelham, 1991).

Taken collectively, we conclude that the formation and/or transport of tubular profiles upon BFA treatment can be explained by the unmasking of microtubule motor attachment sites that are normally covered by coat proteins (Donaldson et al., 1990; Duden et al., 1991; Serafini et al., 1991; Waters et al., 1991; Pelham, 1991). According to this view, the ex-

tent of tubulation of an organelle is inversely related to the level of coat assembly (Klausner et al., 1992). Coat proteins may prevent the interaction of kinesin with a particular organelle, and the various disruptive conditions used here may uncover motor attachment sites and use kinesin for their anterograde transport.

KHC suppression does not prevent the BFA-induced redistribution of the Golgi apparatus, as revealed by the use of markers of the *cis*- and *trans*-Golgi compartments. Since this phenomenon is microtubule- and energy-dependent in several cell types (reviewed in Klausner et al., 1992), including nerve cells (Feiguin, F., and A. Caceres, unpublished observations), motor proteins other than kinesin may be involved in the normal and BFA-induced transport from the Golgi complex into the ER. The recent cloning of several kinesin-like proteins from murine brain tissue (Aizawa et al., 1992) should help determine if anterograde microtubule-based motors participate in this important transport event in nerve cells. Interestingly, transport from the Golgi to ER does not have an absolute requirement for microtubules; therefore, the collapse of the ER to the cell center where the Golgi resides may bring these structures into proximity and circumvent the requirement for microtubules in Golgi to ER traffic.

Kinesin in the Endocytic Pathway

The overall translocation of various endocytic vesicles from a peripheral to a perinuclear location depends on intact microtubules (DeBrabander et al., 1988; Gruenberg and Howell, 1989; Bomsel et al., 1990). LY accumulates in late endosomes, which may interact with microtubules via kinesin and dynein (Parton et al., 1991). The perinuclear location of these organelles implies that the dominant motor responsible for normal endocytic progression of LY may be a retrograde motor (Matteoni and Kreis, 1987). However, under certain experimental conditions, such as low pH, these organelles can be induced to move "in reverse." When KHC was suppressed, LY-labeled organelles did not undergo a pH-induced redistribution to the processes. These organelles may carry both anterograde and retrograde motors, but maintain their perinuclear location by inhibiting kinesin. Alternatively, the low pH may engage an oppositely directed motor by inducing attachment to kinesin or detachment from dynein. When a peripherally directed movement is induced by the pH shift, a latent kinesin activity is revealed. In contrast to the ER, a retrograde motor is likely to dominate in maintaining the cytological locus of late endosomes. However, related organelles in cell types other than those used here may use an oppositely directed motor as dominant. For example, the tubular lysosomes of murine macrophages collapse centrally after the inhibition of KHC with antibodies (Hollenbeck and Swanson, 1990).

Given the microtubule organization of most cells, microtubule motors will maintain organelles in a perinuclear location with retrograde motors, and in a peripheral location with anterograde motors. As described in the manipulations here, some organelles can be displaced from their normal cellular loci with drug treatments or by altering the pH. Displacements of late endosomes to the periphery of astrocytes or to the processes of neurons after a reduction in pH represents a translocation to a site accessible only via an anterograde motor (assuming that microtubules do not reorient). One conclusion from these observations is that late endosomes have the capacity for bidirectional movement, but they use predominantly a retrograde motor. Therefore, the regulation of appropriate motor activity in cells involves both the activation and suppression of motors to maintain the compartmentation of specific organelles.

Finally, conventional KHC represents only one member of the kinesin superfamily. Because the known members of this superfamily have translation initiation codons and 5′ untranslated sequences that are not highly conserved (Niclas et al., 1994; and for reviews see Goldstein, 1991; Endow and Titus, 1992) and that differ from the antisense oligonucleotide sequences used here, one would not expect a global loss of motor function. KHC suppression did not induce the complete cessation of organelle translocation, nor was the punctate pattern of vital labeling by DiOC6(3) altered. This discrete punctate DiOC6(3) labeling, which presumably represents mitochondria and other vesicular organelles within areas devoid of reticular staining, did not differ from controls. Furthermore, labeling of KHC-suppressed cells with LY also revealed intact transport in the endocytic pathway, beginning with internalization of the marker and its subsequent accumulation in late endosomes in the cell body.

The authors are indebted to Dr. Brian Burke (Harvard Medical School, Boston, MA) and Bernard Hoflack (European Molecular Biology Laboratory, Heidelberg, Germany) for providing some of the antibodies used in this study.

This work was supported by a Fogarty International Grant (TW00137-02) and by grants from CONICET, CONICOR, and Fundacion Antorchas to A. Caceres. F. Feiguin is a predoctoral fellow from the National Council of Research from Argentina (CONICET).

Received for publication 9 June 1994 and in revised form 10 August 1994.

References

Aizawa, H., Y. Sekine, R. Takemura, Z. Zhang, M. Nangaku, and N. Hirokawa. 1992. Kinesin family in murine central nervous system. *J. Cell Biol.* 119:1287–1296.

Banker, G. A. 1980. Trophic interactions between astroglial cells and hippocampal neurons in culture. *Science (Wash. DC).* 209:809–810.

Bomsel, M., K. Prydz, R. G. Parton, J. Gruenberg, and K. Simons. 1989. Endocytosis in filter grown Madin-Darby canine kidney cells. *J. Cell Biol.* 109:3243–3258.

Brady, S. T. 1985. A novel brain ATPase with properties expected for the fast axonal transport motor. *Nature (Lond.).* 317:73–75.

Brady, S. T., K. K. Pfister, and G. S. Bloom. 1990. A monoclonal antibody against the heavy chain of kinesin inhibits both anterograde and retrograde axonal transport in isolated squid axoplasm. *Proc. Natl. Acad. Sci. USA.* 81:1061–1065.

Brady, S. T., and K. K. Pfister. 1991. Kinesin interactions with membrane bound organelles in vivo and in vitro. *J. Cell Sci.* 14(Suppl.):103–108.

Caceres, A., J. Mautino, and K. S. Kosik. 1992. Suppression of MAP-2 in cultured cerebellar macroneurons inhibits minor neurite formation. *Neuron.* 9:607–618.

Cooper, M. S., A. H. Cornell-Bell, A. Chernjavsky, J. W. Dani, and S. J. Smith. 1990. Tubulovesicular processes emerge from Trans-Golgi cisternae, extend along microtubules and interlink adjacent Trans-Golgi elements into a reticulum. *Cell.* 61:135–145.

Dabora, S. L., and M. P. Sheetz. 1988. The microtubule-dependent formation of a tubulovesicular network with characteristics of the ER from cultured cell extracts. *Cell.* 54:27–35.

Dailey, M., and P. C. Bridgman. 1989. Dynamics of the endoplasmic reticulum and other membranous organelles in growth cones of cultured neurons. *J. Neurosci.* 9:1897–1909.

DeBrabander, M. J., R. Nuydens, H. Geerts, and C. R. Hopkins. 1988. Dynamic behaviour of the transferrin receptor followed in living epidermoid carcinoma (A431) cells followed with nanovid microscopy. *Cell Motil. Cytoskel.* 9:30–47.

Damke, H., J. Klumperman, K. von Figura, and T. Braulke. 1991. Effects of brefeldin A on the endocytic route. *J. Biol. Chem.* 266:24829–24833.

Donaldson, J. G., J. Lippincott-Schwartz, and R. D. Klausner. 1991. Guanine nucleotides modulate the effects of Brefeldin A in semipermeable cells: regulation of the association of a 110-kD peripheral membrane protein with the

Golgi apparatus. *J. Cell Biol.* 112:579–588.
Dotti, C. G., C. Sullivan, and G. A. Banker. 1988. The establishment of polarity by hippocampal neurons in culture. *J. Neurosci.* 8:1454–1468.
Duden, R., G. Griffiths, R. Frank, P. Argos, and T. E. Kreis. 1991. β-COP, a 110-kd protein associated with non-clathrin-coated vesicles and the Golgi complex, shows homology to β-adaptin. *Cell.* 64:649–665.
Endow, S. A., and M. Titus. 1992. Genetic approaches to molecular motors. *Annu. Rev. Cell Biol.* 8:29–66.
Fath, K. R., G. M. Trimbur, and D. R. Burgess. 1994. Molecular motors are differentially distribution on Golgi membranes from polarized epithelial cells. *J. Cell Biol.* 126:661–675.
Ferreira, A., J. Niclas, R. D. Vale, G. A. Banker, and K. S. Kosik. 1992. Suppression of kinesin expression in cultured hippocampal neurons using antisense oligonucleotides. *J. Cell Biol.* 117:595–606.
Ferreira, A., A. Caceres, and K. S. Kosik. 1993. Intraneuronal compartments of the amyloid precursor protein. *J. Neurosci.* 13:3112–3123.
Gho, M., K. McDonald, B. Ganetzky, and W. M. Saxton. 1992. Effects of kinesin mutations on neuronal functions. *Science (Wash. DC).* 258:313–316.
Goldstein, L. S. B. 1991. The kinesin superfamily: tails of functional redundancy. *Trends Cell Biol.* 1:93–98.
Griffiths, G., B. Hoflack, K. Simons, I. Mellman, and S. Kornfeld. 1988. The mannose 6-phosphate receptor and the biogenesis of lysosomes. *Cell.* 52:329–341.
Gruenberg, J., and K. E. Howell. 1989. Membrane traffic in endocytosis: insights from cell-free assays. *Annu. Rev. Cell Biol.* 5:453–481.
Hall, D. H., and E. M. Hedgecock. 1991. Kinesin-related gene unc-104 is required for axonal transport of synaptic vesicles in *C. elegans*. *Cell.* 65: 837–847.
Henson, J. H., D. Nesbitt, B. D. Wright, and J. M. Scholey. 1992. Immunolocalization of kinesin in sea urchin coelomocytes. Association of kinesin with intracellular organelles. *J. Cell Sci.* 103:309–320.
Hirokawa, N., R. Satyoshitabe, N. Kobayashi, K. K. Pfister, G. S. Bloom, and S. T. Brady. 1991. Kinesin associates with anterogradely transported membrane organelles in vivo. *J. Cell Biol.* 114:295–302.
Hollenbeck, P. J. 1989. The distribution, abundance and subcellular localization of kinesin. *J. Cell Biol.* 108:2335–2342.
Hollenbeck, P. J., and L. A. Swanson. 1990. Radial extensions of macrophage tubular lysosomes supported by kinesin. *Nature (Lond.).* 346:864–866.
Keith, C. H. 1991. Quantitative fluorescent techniques for the determination of local microtubule polymerization equilibria in cultured neurons. *J. Neurosci. Methods.* 39:141–152.
Klausner, R. D., J. G. Donaldson, and J. Lippincott-Schwartz. 1992. Brefeldin A: insights into the control of membrane traffic and organelle structure. *J. Cell Biol.* 116:1071–1080.
Leopold, P. L., A. W. McDowall, K. K. Pfister, G. S. Bloom, and S. T. Brady. 1992. Association of kinesin with characterized membrane-bounded organelles. *Cell Motil. Cytoskel.* 23:19–33.
Lim, S. S., K. J. Edson, P. C. Letourneau, and G. O. Borisy. 1990. A test of microtubule translocations during neurite elongation. *J. Cell Biol.* 111: 123–130.
Lippincott-Schwartz, J., L. C. Yuan, J. S. Bonifacino, and R. D. Klausner. 1989. Rapid redistribution of Golgi proteins into the ER in cells treated with Brefeldin A: evidence for membrane cycling from Golgi to ER. *Cell.* 56:801–813.
Lippincott-Schwartz, J., J. G. Donaldson, A. Schweizer, E. G. Berger, H. P. Hauri, L. C. Yuan, and R. D. Klausner. 1990. Microtubule-dependent retrograde transport of proteins into the ER in the presence of Brefeldin A suggests an ER recycling pathway. *Cell.* 60:821–836.
Lipsky, N. G., and R. E. Pagano. 1985. A vital stain for the Golgi apparatus. *Science (Wash. DC).* 228:745–747.
Matteoni, R., and T. E. Kreis. 1987. Translocation and clustering of endosomes and lysosomes depends on microtubules. *J. Cell Biol.* 105:1253–1265.
Navone, F., J. Niclas, N. Hom-Booher, L. Sparks, H. D. Bernstein, G. McGaffrey, and R. D. Vale. 1992. Cloning and expression of a human heavy chain gene: interaction of the COOH-terminal domain with cytoplasmic microtubules in transfected CV-1 cells. *J. Cell Biol.* 117:1265–1275.
Niclas, J., F. Navone, N. Hom-Booher, and R. D. Vale. 1994. Cloning and localization of a conventional kinesin motor expressed exclusively in neurons. *Neuron.* 12:1059–1072.
Pagano, R. E., M. A. Sepanski, and O. C. Martin. 1989. Molecular trapping of a fluorescent analogue at the Golgi apparatus of fixed cells: interactions with endogenous lipids provides a *trans*-Golgi marker for both light and electron microscopy. *J. Cell Biol.* 109:2067–2080.
Parton, R. G., C. G. Dotti, R. Bacallao, I. Kurtz, and K. Prydz. 1991. pH-induced microtubule-dependent redistribution of late endosomes in neuronal and epithelial cells. *J. Cell Biol.* 113:261–274.
Pelham, H. R. B. 1991. Multiple targets for Brefeldin A. *Cell* 67:449–451.
Porter, M. E., J. M. Scholey, D. L. Stemple, G. P. A. Vigers, R. D. Vale, R., M. P. Sheetz, and J. R. McIntosch. 1987. Characterization of the microtubule movement produced by sea urchin egg kinesin. *J. Biol. Chem.* 262:2794–2802.
Scholey, J. M., M. E. Porter, P. M. Grissom, and J. R. McIntosh. 1985. Identification of kinesin in sea urchin eggs, and evidence for its localization in the mitotic spindle. *Nature (Lond.).* 318:483–486.
Serafini, T., G. Stenbeck, A. Brecht, F. Lottspeich, L. Orci, J. E. Rothman, and F. T. Wieland. 1991. A coat subunit of Golgi-derived non-clathrin-coated vesicles with homology to the clathrin coated vesicle coat protein β-adaptin. *Nature (Lond.).* 349:215–220.
Terasaki, M., J. Song, M. Wong, M. Weiss, and L. B. Chen. 1984. Localization of endoplasmic reticulum in living and glutaraldehyde fixed cells with fluorescent dyes. *Cell.* 38:101–108.
Toyoshima, I., H. Yu, E. Steuer, and M. P. Sheetz. 1992. Kinectin, a major kinesin-binding protein on ER. *J. Cell Biol.* 118:1121–1131.
Vale, R D., and H. Hotani. 1988. Formation of membrane networks in vitro by kinesin-driven microtubule movement. *J. Cell Biol.* 107:2233–2241.
Vale, R. D., T. S. Reese, and M. P. Sheetz. 1985*a*. Identification of a novel force generating protein, kinesin, involved in microtubule-based motility. *Cell.* 42:39–50.
Vale, R. D., B. J. Schnapp, T. J. Mitchison, E. Steuer, T. S. Reese, and M. P. Sheetz. 1985*b*. Different axoplasmic proteins generate movement in opposite directions along microtubules in vitro. *Cell.* 43:623–632.
Waters, M. G., T. Serafini, and J. E. Rothman. 1991. "Coatomer": a cytosolic protein complex containing subunits of non-clathrin-coated Golgi transport vesicles. *Nature (Lond.).* 349:248–251.
Wood, S. A., J. E. Park, and W. J. Brown. 1991. Brefeldin A causes a microtubule-mediated fusion of the trans-Golgi network and early endosomes. *Cell.* 67:591–600.